Predictive modelling of the properties and toughness of polymeric materials, Part I: Why is polystyrene brittle and polycarbonate tough?

JOURNAL OF MATERIALS SCIENCE **35** (2000) 2855–2867

Predictive modelling of the properties and toughness of polymeric materials

Part I *Why is polystyrene brittle and polycarbonate tough?*

R. J. M. SMIT*, W. A. M. BREKELMANS, H. E. H. MEIJER
Materials Technology (MaTe), Dutch Polymer Institute (DPI), Eindhoven University of Technology (TUE), P.O. Box 513, 5600 MB Eindhoven, The Netherlands
E-mail: Robert.Smit@unilever.com

The brittleness of polystyrene (PS) and the toughness but notch sensitivity of polycarbonate (PC) have been studied by the detailed finite element analyses of the stress and strain fields in a notched tensile bar with a minor defect. The defect represented a flaw or imperfection, generated during the test specimen production. The large-strain mechanical responses of both materials were approximated by an accurate elasto-viscoplastic constitutive model with appropriate material parameters. It was assumed that failure occurs instantaneously once the dilative stress exceeds a certain critical craze-initiation stress. The analyses show that the unstable post-yield mechanical response of both materials results in localisation of stresses and strains near the defect at a very low macroscopic strain (0.16%). As a result, a strong dilative stress concentration is formed just below the surface of the defect. For the polystyrene specimen, the critical stress is reached at the defect. For the polycarbonate, however, the effect of the stress concentrating defect was counteracted by a higher craze-initiation stress and stronger strain hardening. The PC craze-initiation resistance, however, did not suffice to overcome the dilative stress concentration raised by the notch tip.

1. Introduction

Using tensile testing as the obvious experimental method, it is generally concluded that polycarbonate (PC) is a ductile material with a macroscopic strain-to-break ε_b equal to 80%, while polystyrene (PS) is brittle with $\varepsilon_b < 2\%$, as shown in Fig. 1. The explanation for this opposite behaviour of those seemingly comparable glassy polymers is usually sought in the experimental observations that PC shear yields and PS crazes.

The macroscopic behaviour, however, is in contrast with the microscopically measured behaviour. For instance in PS craze fibrils bridging craze surfaces, it has been observed that polystyrene deforms in a ductile way, with a maximum fibrilar draw ratio $\lambda_{max} = 4$ (300% linear strain), while the maximum microscopic deformation in the shear bands of polycarbonate is relatively more limited with $\lambda_{max} = 2$ (100% linear strain, see e.g. Kramer [1]). Henkee and Kramer [2] demonstrated that this maximum local strain can be predicted, and thus expected, from the molecular network structure. They revealed that there exists an excellent correlation between the microscopically measured maximum extension ratio λ_{max} and the theoretical maximum extension ratio λ^*_{max} of a single strand in the polymer entanglement network, which is given by

$$\lambda^*_{max} = \frac{l_e}{d} \tag{1}$$

where l_e is the chain contour length between entanglements, which is proportional to the molecular weight M_e between entanglements, and d is the root-mean-square distance between entanglement points, which is proportional to $\sqrt{M_e}$. Those quantities are for polystyrene $l_e \approx 40$ nm, $d \approx 9.6$ nm, $\lambda^*_{max} \approx 4$, and for polycarbonate $l_e \approx 11$ nm, $d \approx 4.4$ nm, $\lambda^*_{max} \approx 2.5$ [1, 3]. These values suggest that polystyrene can be deformed to much higher strains than polycarbonate because of its larger entanglement distance, which is caused by the relative stiffness of the molecular chains, yielding a relatively low entanglement density. The question arises how the macroscopic deformability and toughness are affected by the interaction between deformations in the microstructure and those in the macrostructure.

Is polycarbonate always tough? The answer is no, since the macroscopic deformability of polycarbonate disappears if a specimen is notched and tested under impact conditions (see, e.g. Fraser and Ward [4]). The

* *Present Address*: Unilever Research Vlaardingen, P.O. Box 114, 3130 AC Vlaardingen, The Netherlands.

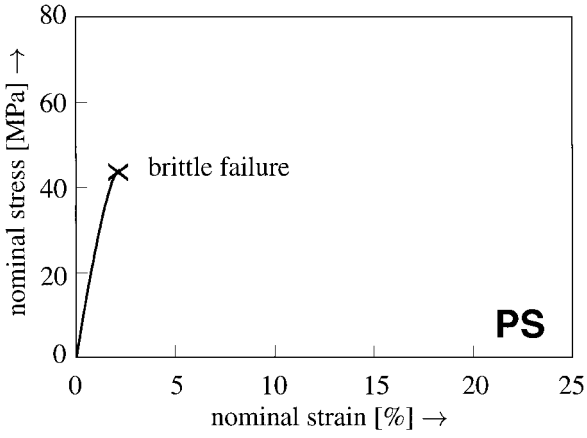

(a)

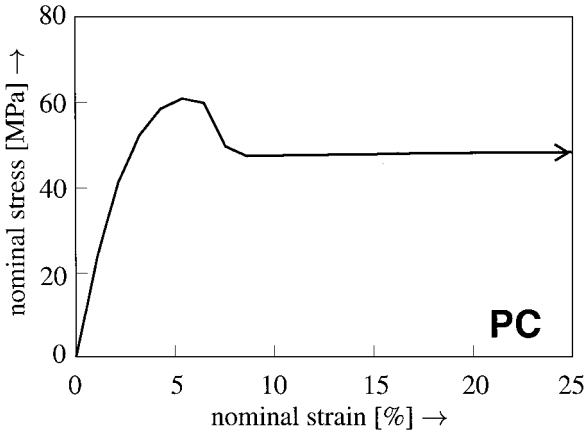

(b)

Figure 1 Typical mechanical responses for (a) polystyrene and (b) polycarbonate measured in uniaxial extension.

toughness can, however, be retrieved by rubber modification and some illustrative examples can be obtained by applying non-adhering core-shell rubbers, where only 5% addition results in a spectacular change from brittle to tough behaviour in notched high-speed tensile tests, see e.g. van der Sanden *et al.* [5]. Hence, polycarbonate can indeed be brittle, but the toughness returns by microstructural modifications.

Is polystyrene always brittle? Recently, a number of authors convincingly proved that polystyrene can also be macroscopically tough and can be manipulated to deform by shear yielding. A drastic increase in strain-to-break was found for different heterogeneous polystyrene systems (multi-layered tapes based on polystyrene-polyphenylene ether (PS-PPE) layers alternating with polyethylene (PE) with a layer thickness of *ca.* 50 nm [6], PS filled with non-adhering core shell rubbers of 200 nm [7] or of 100 nm [8]). In all those systems a transition from (multiple) crazing to complete shear yielding was observed at a certain critical local thickness (either tape thickness or ligament thickness). Magalhães and Borggreve [9] revealed, using X-ray scattering experiments, that the major deformation mechanism in rubber modified polystyrene can be shear yielding, which again demonstrates that the intrinsic toughness of PS can be retrieved on a macroscale by changing the microstructure.

A different, rather academic but nevertheless intriguing method to improve the macroscopic toughness of

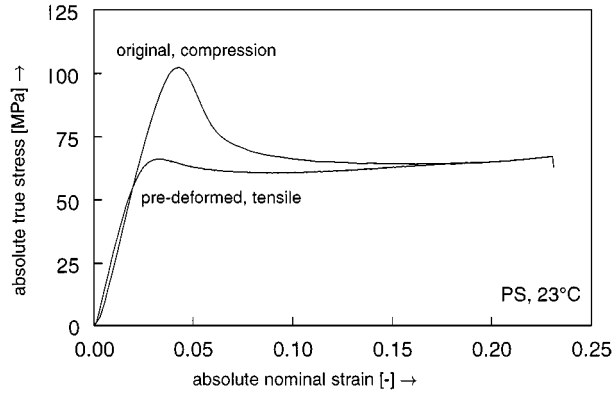

Figure 2 Stress-strain responses for untreated and pre-treated polystyrene, measured during uniaxial compression and uniaxial extension respectively. The pre-treated and subsequently tested specimen is shown in Fig. 3.

polystyrene drastically is the application of compressive pre-deformation [10]. Such a pre-treatment temporary changes the yield behaviour of the specimen, while its molecular structure is retained and no pronounced molecular orientation is introduced [3, 11]. Fig. 2 shows the intrinsic true stress-strain responses of untreated and pre-treated polystyrene, measured in compression† and extension, respectively. The effect of the pre-deformation is clear: the yield stress has been reduced dramatically, the strain softening, which is the stress drop after yield, has been diminished, and the macroscopic strain-to-break in tensile testing has increased from <2% (see Fig. 1a) to a value of 23%. Since the intrinsic strain softening is known to be the main cause of unstable deformation behaviour, often resulting in necking or shear band formation, the elimination of softening causes a more stable macroscopic mechanical behaviour. The consequences for the pre-treated tensile specimen shown in Fig. 2 are twofold: a drastically higher strain-to-break and a nearly homogeneous sample deformation without any neck formation (see the deformed sample in Fig. 3, which is actually fractured). The improvement is, however, only temporary since enhanced physical aging restores the higher yield stress and combined softening, and after *ca.* 15 minutes the pre-treated sample is brittle again (the same phenomena have been found for other amorphous polymers, however, with substantially different time scales for aging: for poly(methyl methacrylate) (PMMA) the brittleness returns after *ca.* 1 day; for polycarbonate the sample necks again (no homogeneous deformation) after *ca.* 3 weeks). These results confirm that reduction of the unstable post-yield strain softening improves the macroscopic deformation behaviour and probably plays a key-role in brittle-to-tough transitions.

Another interesting way to investigate the relationship between (post-)yield response and mechanical behaviour is uniaxial tensile testing at different test temperatures. Fig. 4a and b shows the results of Jansen

† It is remarked that the intrinsic mechanical behaviour of untreated polystyrene cannot be measured in uniaxial extension, because craze formation results in early failure, as is show in Fig. 1a.

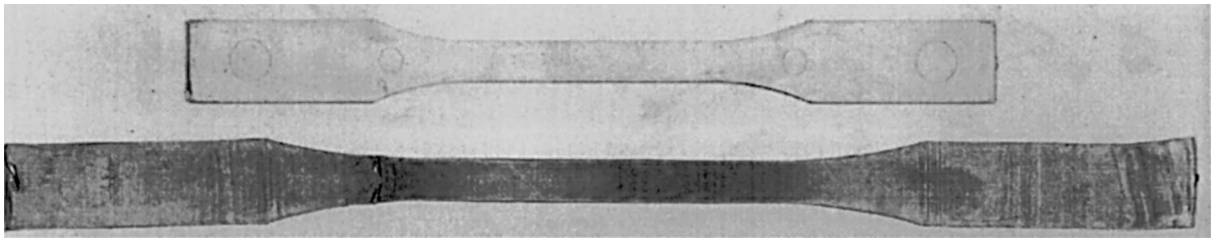

Figure 3 Untreated undeformed tensile specimen (top) and the pre-treated and subsequently tested (bottom) tensile specimen which was pre-conditioned in rolling. The pre-treated sample deformed homogeneously until fracture at a macroscopic strain of approximately 23%.

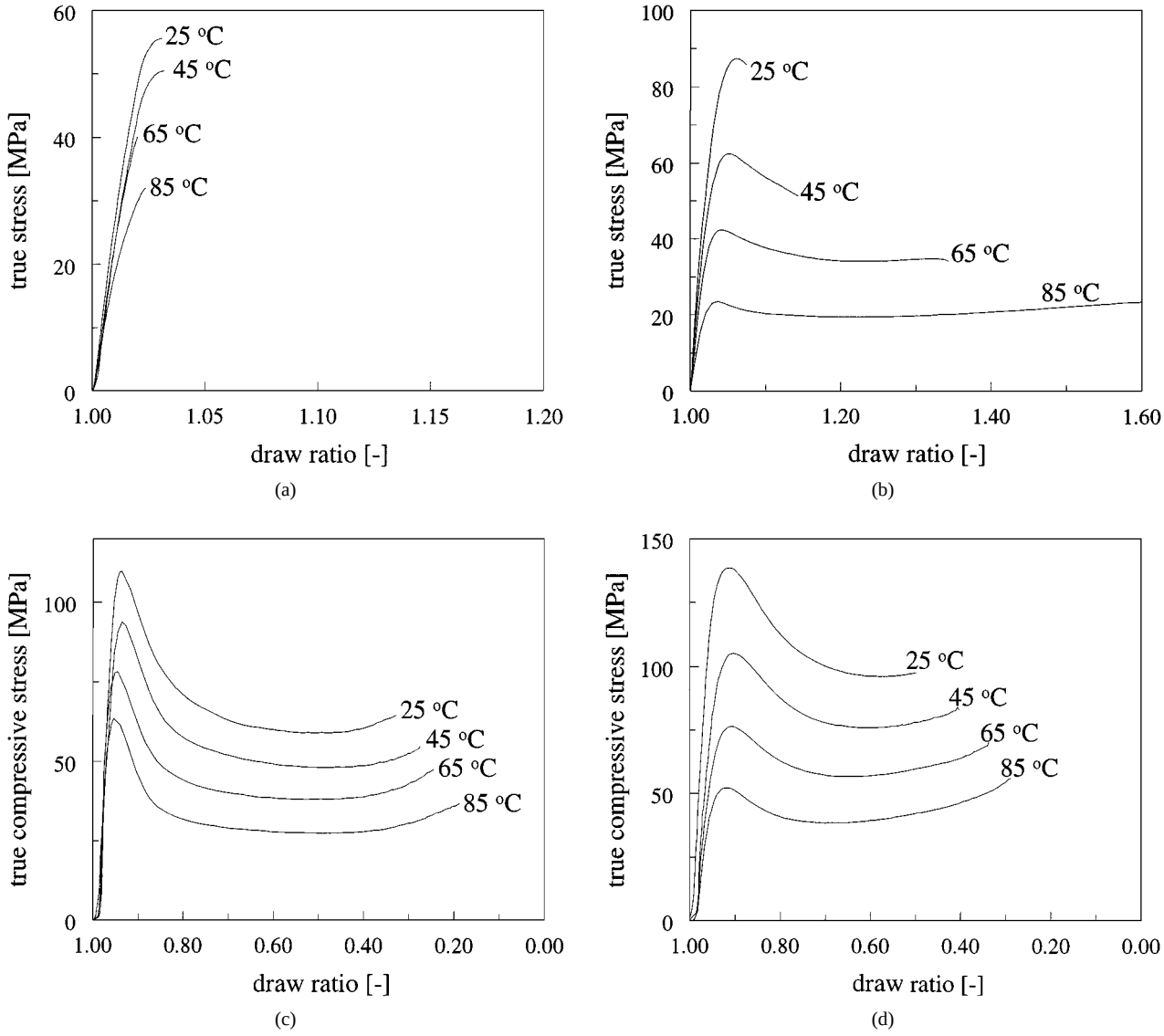

Figure 4 Stress-strain responses for polystyrene (left) and poly(methyl methacrylate) (right) measured in uniaxial extension (top) and uniaxial compression (bottom) at different test temperatures (Reproduced, with permission, from Jansen [12]).

[12] of tensile tests on homogeneous dumb-bell shaped PS and PMMA test specimen at 25, 45, 65 and 85 °C. The temperature influences, of course, the yield stresses of both materials but, more important, the strain-to-break of PMMA remarkably increases with temperature (from 10% at 25 °C up to >60% at 85 °C), while that of polystyrene decreases. A possible reason for this contrasting behaviour can be found in Fig. 4c and d, which depicts the intrinsic mechanical response of both materials, measured in uniaxial compression. Apparently, the stability of the post-yield behaviour of PMMA improves with temperature: the relative stress drop by strain softening reduces from 31% at 25 °C to 27% at 85 °C (stress differences are scaled with the corresponding yield stresses) and the -stabilising- hardening sets in earlier, from a compressive strain of 43% at 25 °C to 32% at 85 °C. The stability of PS gets worse with increasing temperature: the stress drop by strain softening increases from 46% to 56%, while the hardening sets in later, from 50% to 55% compressive strain. These results suggest that the improved stability is responsible for the higher strain-to-break of PMMA at 85 °C.

This is again a strong indication that there indeed exists an important relationship between stability of the post-yield response and ductility.

Summarising, polystyrene is potentially a tough material (while polycarbonate is only moderately tough). Both materials can be brittle at room temperature and their intrinsic toughness can be regained by appropriate microstructural modifications. Furthermore, macroscopic toughness is strongly affected by the stability of the macroscopic (post-)yield behaviour of the material. Despite the fact that this knowledge is known for many years, no general methodology for (even qualitative) toughness predictions for arbitrary shaped heterogeneous polymeric structures is available today. This is caused by three interacting features that are characteristic for the deformation behaviour of heterogeneous polymeric systems, i.e. (i) the intrinsic mechanical behaviour of the individual polymeric components is rather complex (large deformations, elasto-viscoplastic behaviour, strain softening followed by hardening, combined with the influence of temperature and deformation rate), (ii) the micro-macro relationship between the properties on user scale (typical length scale 1–10 mm) and morphological scale (typical length scale 10^{-6}–10^{-3} mm) is unclear, and (iii) the microstructural geometry is usually complex.

It is the ultimate goal of this research to fundamentally understand why polystyrene is brittle, polycarbonate is tough and why rubber toughening works. Foregoing publications presented a generally applicable homogenisation method to solve the micro-macro problem [13], and a modelling approach to investigate the (considerable!) influence of morphological geometry on macroscopic response [14]. The present paper discusses the intrinsic mechanical behaviour of PS and PC and the critical material parameters that may explain the brittleness of polystyrene and the large (uniaxial) strain-to-break but notch sensitivity of polycarbonate. Two subsequent papers study the effects of microstructural modifications on the macroscopic mechanical response (Part II [15]) and on the defect and notch sensitivity of notched tensile bars of heterogeneous PS and PC (Part III [16]).

The outline of this paper is as follows. The intrinsic mechanical behaviour of homogeneous polystyrene and polycarbonate is examined first. Then, the recently developed generalised compressible single-mode Leonov model is introduced, a model fit of the measured intrinsic behaviour is presented, and the selection of a crack criterion is discussed. Finally, the generalised compressible Leonov model and the crack criterion are applied in a finite element model of a notched tensile bar, with an additional imperfection located at the notch tip, in order to investigate the physical reasons for the brittleness of PS and notch sensitivity and toughness of PC.

2. Intrinsic mechanical behaviour of polystyrene and polycarbonate

The main features of the large-strain intrinsic mechanical response of an amorphous glassy polymer can be captured by uniaxial compression experiments, where homogeneous sample deformations can be achieved up to large strains (see, e.g. Hasan *et al.* [17]). Fig. 5 visualises the compressive stress-strain curves of homogeneous polystyrene and polycarbonate. The responses of both materials show the typical mechanical behaviour that is representative for a range of glassy polymers: a small-strain (visco-)elastic response, followed by yield, intrinsic strain softening and subsequent strain hardening. Both materials have a comparable Young's modulus and yield stress but a different post-yield response: polystyrene exhibits a strong strain softening followed by minor hardening (with a hardening modulus of *ca.* 12 MPa), resulting in an unstable post-yield deformation behaviour until the hardening sets in, while polycarbonate shows less softening and more (stabilising) hardening (with a modulus of *ca.* 29 MPa) and, consequently, a relatively stable behaviour. Since in particular strain softening and hardening distinguish, qua intrinsic yield behaviour, polycarbonate from polystyrene, a further elaboration on the fundamental nature of those phenomena is adequate.

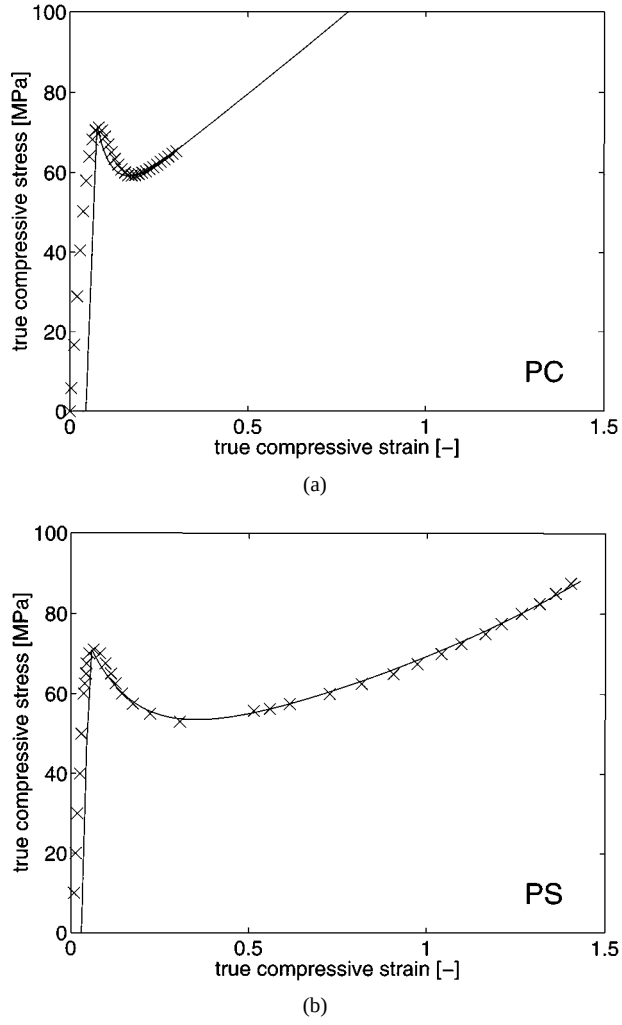

Figure 5 True compressive stress versus true strain measured during uniaxial compression at a strain rate of $-0.001\ s^{-1}$ for (a) quenched polycarbonate and (b) quenched polystyrene, tested at room temperature. The marks represent the experimental data from Hasan *et al.* [17] and Timmermans [18], the solid lines result from the constitutive modelling. The stress ordinates of the model fits are shifted in order to obtain a closer approximation of the yield and post-yield response.

The molecular configuration of a glassy polymer is essentially the same as it was in the melt from which it solidified, and can be envisaged as a random assembly of entangled covalently bonded chains, held together by secondary forces. The relatively weak secondary bonds are responsible for the initial (visco-)elastic behaviour, yield and strain softening. Strain softening is, therefore, closely related to the yield and pre-yield viscoelastic response. Modifying the yield behaviour by, for example, a thermal or mechanical pre-treatment consequently results in an altered softening behaviour, see e.g. Fig. 2 (more examples can be found in the literature, especially in the work of Hasan *et al.* [17], who effectively manipulated the yield and strain softening behaviour of polystyrene by quenching and annealing). Strain hardening, on the contrary, originates from the rubber-elastic response of the entanglement network and is thus not related to the yield and softening behaviour. Notice that this implies that the molecular structure not only determines the maximum network extension (see Equation 1) but also the strain hardening response. Using the Gaussian approximation of the rubber elasticity theory, it can easily be deduced that the hardening modulus H scales with d^{-2} ($H \sim M_e^{-1}$, $d \sim \sqrt{M_e}$, so $H \sim d^{-2}$), which elucidates the important difference between the hardening responses of polycarbonate and polystyrene (PC: $H \approx 29$ MPa, $d \approx 4.4$ nm; PS: $H \approx 12$ MPa, $d \approx 9.6$ nm; values for d adopted from Kramer [1]). So the impressive intrinsic ductility of polystyrene goes hand in hand with a rather disappointing strain hardening behaviour.

3. Constitutive modelling

The different origins of the deformation contributions are reflected in the three-dimensional (3D) phenomenological constitutive model employed as two parallel parts, i.e. the response originating from the weak secondary forces, which include (visco-)elasticity, yield and strain softening, and the response that results from the entanglement network, the strain hardening response [11, 18]. The first part of this so-called generalised compressible Leonov model is a compressible elasto-viscoplastic model, essentially a Maxwell 'spring-dashpot' model with an Eyring viscosity [19], extended with strain softening according to Hasan *et al.* [17]. The second part is described by a simple neo-Hookean spring. Tervoort [11] and Timmermans [18] demonstrated that this model is capable of accurately capturing the influence of strain rate and temperature on the yield and post-yield response of glassy polycarbonate in tensile, compression and shear testing. Timmermans [18] compared the generalised single-mode Leonov model with similar models of Boyce *et al.* [20–22] and Wu and van der Giessen [23], who modelled the strain hardening part according to a Langevin approach, and concluded that all the models produce comparable results. The advantage of the generalised Leonov model, however, is its potential ability to accurately describe the nonlinear viscoelastic region with a multi-mode version (18 'spring-dashpots' in parallel [24]). In the present study, which mainly focuses on post-yield behaviour, only a single-mode constitutive model was used for computational reasons. In the following the governing constitutive equations are summarised.

In the generalised Leonov model [19] extended with softening and hardening, the Cauchy stress $\boldsymbol{\sigma}$ is additively decomposed in an effective stress $\boldsymbol{s}$ and a hardening stress $\boldsymbol{r}$, according to

$$\boldsymbol{\sigma} = \boldsymbol{s} + \boldsymbol{r} \tag{2}$$

The effective stress $\boldsymbol{s}$ is described by a (compressible) generalisation of the originally incompressible Leonov model [25], proposed by Baaijens [26]. The generalised compressible Leonov model is based on the multiplicative decomposition of the actual deformation gradient tensor $\boldsymbol{F}$ in a volumetric part $J^{\frac{1}{3}}\boldsymbol{I}$, an isochoric elastic part $\boldsymbol{F}_e$, and a (by definition isochoric) plastic part $\boldsymbol{F}_p$, according to

$$\boldsymbol{F} = J^{\frac{1}{3}}\boldsymbol{I} \cdot \boldsymbol{F}_e \cdot \boldsymbol{F}_p \tag{3}$$

where $\boldsymbol{I}$ denotes the identity tensor and with

$$J = \det(\boldsymbol{F}) \tag{4}$$

while $\boldsymbol{F}_p$ defines the state that would instantaneously be recovered if all the loads were suddenly removed from the sample, fictitiously assuming that the hardening can be left out of consideration. If it is postulated that the total spin tensor equals the elastic spin tensor, it can be proved that the elastic shape deformation, defined by the isochoric elastic left Cauchy-Green deformation tensor

$$\boldsymbol{B}_e = \boldsymbol{F}_e \cdot \boldsymbol{F}_e^c \tag{5}$$

(the superscript c indicates conjugation) is given by the following rate equation:

$$\overset{\triangledown}{\boldsymbol{B}}_e = -\boldsymbol{D}_p \cdot \boldsymbol{B}_e - \boldsymbol{B}_e \cdot \boldsymbol{D}_p \tag{6}$$

In this equation, $\boldsymbol{D}_p$ represents the plastic strain rate tensor and the upper triangle defines the isochoric Truesdell objective rate as

$$\overset{\triangledown}{\boldsymbol{B}}_e = \dot{\boldsymbol{B}}_e - \boldsymbol{L}^d \cdot \boldsymbol{B}_e - \boldsymbol{B}_e \cdot (\boldsymbol{L}^d)^c \tag{7}$$

where $\boldsymbol{L}$ is the velocity gradient tensor and the superscript d denotes the deviatoric part. Assuming only small volumetric deformations, the deviatoric part $\boldsymbol{s}^d$ of the effective stress $\boldsymbol{s}$ is related to $\boldsymbol{B}_e^d$ through the generalised Hookean relation

$$\boldsymbol{s}^d = G\boldsymbol{B}_e^d \tag{8}$$

where G represents the shear modulus. The hydrostatic part of the effective stress $\boldsymbol{s}^h$ is coupled to the volume change by

$$\boldsymbol{s}^h = \kappa(J-1)\boldsymbol{I} \tag{9}$$

with κ the bulk modulus.

The hardening stress is described by a simple neo-Hookean model [11, 18]

$$\boldsymbol{r} = H\tilde{\boldsymbol{B}}^{\mathrm{d}} \tag{10}$$

where H is the strain hardening modulus, and $\tilde{\boldsymbol{B}}$ represents the isochoric left Cauchy-Green strain tensor, defined as

$$\tilde{\boldsymbol{B}} = J^{-\frac{2}{3}}\boldsymbol{F}\cdot\boldsymbol{F}^{\mathrm{c}} \tag{11}$$

The generalised compressible Leonov model is completed by expressing the dissipative plastic strain rate $\boldsymbol{D}_{\mathrm{p}}$ in the effective stress $\boldsymbol{s}$. Tervoort *et al.* [19] proposed to use a generalised Newtonian flow rule with a stress dependent Eyring viscosity η, to relate the plastic deformation rate to the deviatoric effective stress as

$$\boldsymbol{D}_{\mathrm{p}} = \frac{\boldsymbol{s}^{\mathrm{d}}}{2\eta} \tag{12}$$

Timmermans [18] completed the model by adding pressure dependence ($p = -\frac{1}{3}\,\mathrm{tr}(\boldsymbol{s})$, where $\mathrm{tr}(\boldsymbol{s})$ denotes the trace of the effective stress) and intrinsic softening effects (D) to the viscosity expression, using a softening evolution equation originally proposed by Hasan *et al.* [17]:

$$\eta = \frac{A_0\, s}{\exp(D - p\mu/\tau_0)\,\sinh(s/\tau_0)},$$
$$s = \sqrt{\mathrm{tr}(\boldsymbol{s}^{\mathrm{d}}\cdot\boldsymbol{s}^{\mathrm{d}})/2}, \quad p = -\frac{1}{3}\,\mathrm{tr}(\boldsymbol{s}) \tag{13}$$

$$\dot{D} = \left(1 - \frac{D}{D_\infty}\right)\frac{hs}{\eta\sqrt{2}} \tag{14}$$

with initially $D = 0$, and with the material parameters: A_0 a time constant, τ_0 a characteristic stress, μ a pressure coefficient, h the softening slope parameter and D_∞ the softening limit. Notice that the softening variable D reduces the viscosity η and thus lowers the effective stress $\boldsymbol{s}^{\mathrm{d}}$ for a certain given plastic strain rate $\boldsymbol{D}_{\mathrm{p}}$ (see Equation 12). The softening evolution equation controls the growth of D: elastic behaviour involves a high viscosity and thus $1/\eta \ll 1$, so D remains approximately constant; yield involves a low viscosity and thus a growth of D up to the limiting value D_∞.

A fit of the compression data for polystyrene and polycarbonate using the generalised compressible Leonov model has been inserted in Fig. 5. Since this single-mode model cannot simulate the pre-yield viscoelastic response accurately, the strain ordinate of the model fit is shifted in order to obtain a closer fit of the yield and post-yield behaviour while using the initial modulus as an elastic modulus. The large-strain uniaxial compression data were supplemented with the strain rate dependent yield stresses measured for different loading geometries in order to determine the influence of strain rate and pressure on yield (PS: planar compression, uniaxial extension under superimposed hydrostatic pressure; PC: planar compression, uniaxial extension [11]). The resulting set of material parameters is given in Table I. Figs 6 and 7 display the model response for polystyrene and polycarbonate in a uniaxial tensile configuration at different strain rates. Apparently, polystyrene shows a more pronounced strain rate dependence than polycarbonate. It is noteworthy that this strain rate dependence stabilises the unstable post-yield deformation behaviour in localisation zones, since fast strain localisations involve high strain rates and, consequently, higher stresses. Hence, this stabilisation mechanism (partially) counteracts the unstable post-yield response that is caused by the strain softening.

The material parameters are used in a robust and accurate fully implicit finite element implementation of

TABLE I Material parameters for polycarbonate (PC) and polystyrene (PS) at room temperature

	Parameters							
	G [MPa]	K [MPa]	A_0 [s]	τ_0 [MPa]	μ [−]	D_∞ [−]	h [−]	H [MPa]
PC	840	3000	4.0×10^{25}	0.72	0.07	19	270	29
PS	1200	4230	4.5×10^{10}	2.062	0.09	8.8	45	12

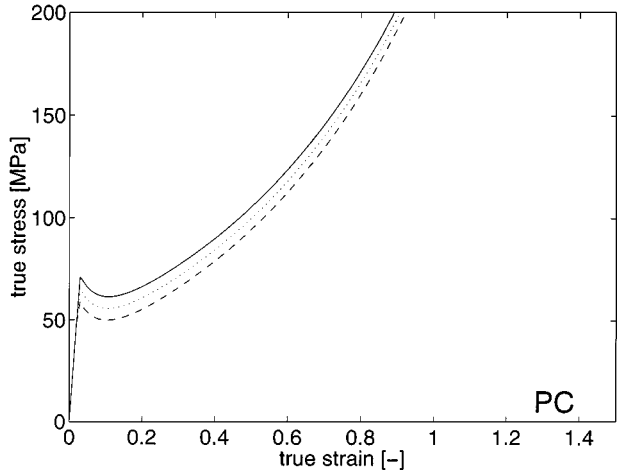

Figure 6 Model predictions of axial stress versus strain for polycarbonate subjected to uniaxial extension at strain rates 10^{-1} s^{-1} (solid), 10^{-3} s^{-1} (dotted), and 10^{-5} s^{-1} (dashed).

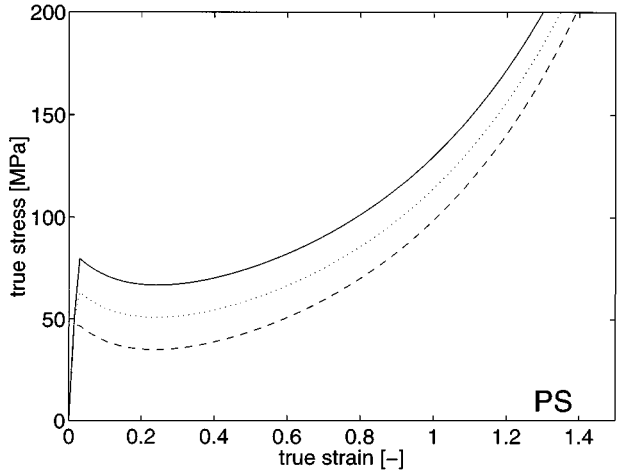

Figure 7 Model predictions of axial stress versus strain for polystyrene subjected to uniaxial extension at strain rates 10^{-1} s^{-1} (solid), 10^{-3} s^{-1} (dotted), and 10^{-5} s^{-1} (dashed).

the model in the commercial finite element code MARC [27], see for more details Reference [28]. The resulting finite element program enables the investigation of the local and global mechanical response of 3D structures of polycarbonate and/or polystyrene, subjected to an arbitrary load history.

4. Selection of a crack-initiation criterion

A simple and rather primitive crack-initiation criterion has been applied: a crack is assumed to be formed instantaneously after the local dilative stress reaches a certain critical value in a region that is shear yielded, provided that the region is large enough to accommodate a craze structure of two or more craze fibrils. This particular choice will be elucidated in the following.

The precise conditions determining craze or crack initiation are, unfortunately, not clarified yet and, therefore, the subject of continuously ongoing research (see, e.g. [11, 29, 30]). One of the most difficult problems is the identification of the nucleation site before the first crack or craze appears. In thermoplastics, the crack nucleus usually starts as a craze [31], and in a number of publications bulk materials were examined, using Scanning and Transmission Electron Microscopy, but no defects could be detected in the material which could act as craze initiators [32]. Because of the unknown location of microscopically small nucleation sites, the local deformation history of the material is not known and, consequently, the conditions that govern craze or crack nucleation are unknown [1].

Many experiments, however, indicate that the dilative stress plays a key role during the nucleation process [1, 32]. Narisawa *et al.* [33] proposed, therefore, to use the critical dilative stress as an empirical criterion for craze or crack nucleation, provided that crazing is preceded by some type of shear yielding. They estimated the critical dilative stress, σ_c, for polystyrene and polycarbonate to be approximately 40 MPa and 90 MPa, respectively [32]. For those estimates an indirect measurement technique was used: the distance of a nucleus from the notch tip was approximated by a visual inspection of the fracture surface, while the dilative stress was determined from the slip-line field (SLF) theory of Hill [34]. The SLF theory, however, assumes that the material is elastic-perfectly plastic without strain hardening, which is probably inappropriate for amorphous glassy polymers featuring intrinsic strain softening and strain hardening. Especially intrinsic strain softening is known to accelerate the localisation of plastic (and thus volume invariant) strains near a stress concentrating defect, which could result in higher triaxial stresses. This might imply that the reported values underestimate the dilative stresses accompanying craze initiation. Similar considerations motivated Nimmer and Woods [35] to compare SLF results with a more accurate 3D finite element analysis of notched polycarbonate bending experiments and they indeed reported important differences between slip-line field predictions and finite element results. As an alternative, they simply calculated the maximum dilative stress in the PC specimen at the moment of craze formation and produced, surprisingly, similar results as Narisawa and Yee [32]: $\sigma_c \approx$ 90–100 MPa. Those results do unfortunately not confirm the accuracy of the estimated critical dilative stress value for the less stable polystyrene and, therefore, the critical value of PS is expected to be in the range of 40–50 MPa.

Using an extremely brittle polystyrene, Govaert and Tervoort [11, 36] convincingly proved that craze initiation is indeed preceded by yield. It is emphasised, however, that craze initiation cannot be considered as a special type of yield, since the craze-initiation stress can depend on the total molecular weight of the polymer [1, 37, 38], while the total molecular weight has no effect on the yield behaviour (which originates from secondary interactions). Notice that this dependence suggests that craze initiation might involve disentanglement of the polymer molecules [38]. Hence, a proper craze-initiation criterion should also take the molecular structure into account.

Since it is outside the scope of the present paper to establish a fully consistent craze-initiation criterion, the approach of Narisawa [33] is adopted, with one extra condition: the region were the craze is formed must be large enough to accommodate a craze structure of two or more craze fibrils (PC: $>$25 nm, PS: $>$50 nm [1]). This condition, which was suggested by Kramer to explain size-induced brittle-to-tough transitions in the thin PS/PPE-PS tapes of van der Sanden *et al.* [6], introduces an absolute length scale in the finite element analysis and is especially important for heterogeneous structures with a very fine morphology (see, e.g., the microstructural analyses in Part II of this series [15]).

5. Prediction of toughness of notched polystyrene and polycarbonate specimens

The toughness of a polymeric material is related to the specific energy consumption before catastrophic failure

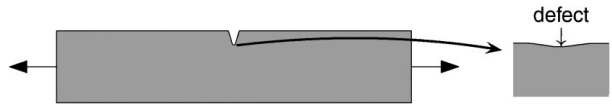

Figure 8 Plane strain model of a notched tensile test specimen with a minor defect at the blunt notch tip.

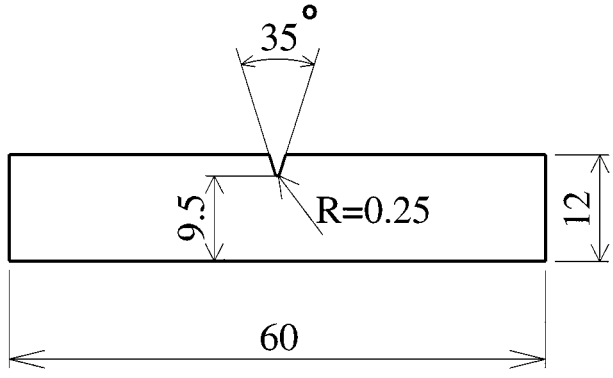

Figure 9 Dimensions (in mm) of the global geometry of the notched tensile test specimen. The geometric imperfection at the bottom of the notch tip is defined as a cosine shaped wave of length $0.04R$ and amplitude $0.002R$.

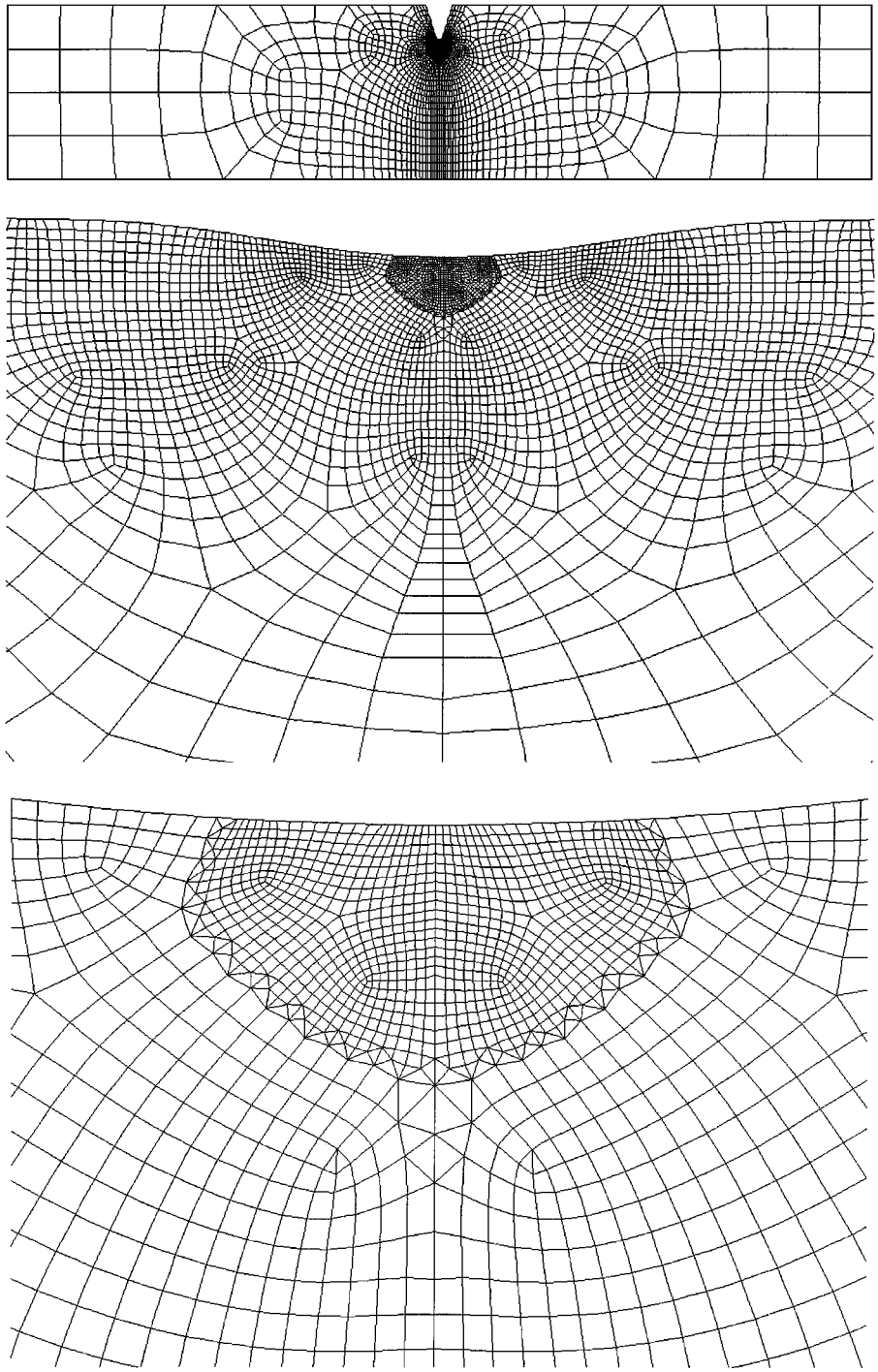

Figure 10 Finite element model of the notched tensile specimen and details of the mesh refinement near the cosine shaped defect.

occurs. Recently, Havriliak *et al.* [39] revealed that most of the impact energy measured during an Izod impact test on notched amorphous (glassy polycarbonate and polyvinylchloride, PVC), and heterogeneous (rubber modified PVC and polycaprolactam, nylon 6) polymers is consumed before the nucleation of the first crack or craze is observed (the energy dissipated during crack propagation can be neglected). This result suggests that toughness of a similar polymeric material is determined by only two items: (a) the moment of crack or craze nucleation and (b) the energy dissipated up to this moment.

In this study, this simplified approach will be adopted to predict the toughness of notched tensile bars of polycarbonate and polystyrene by detailed finite element modelling. This particular strategy enables us to avoid the extremely complex and yet unsolved problem of crack propagation. The moment of crack or craze nucleation is determined by the critical dilative stress criterion, discussed in the previous section. The energy consumption by elastic or plastic deformation can be estimated from the evolving stress and strain fields, as predicted by the finite element analyses.

A plane strain notched test specimen is considered with a small 'geometric' imperfection at the root of the blunt notch tip, as shown in Fig. 8, where the imperfection represents a flaw or a manufacturing defect. The dimensions of the specimen are depicted in Fig. 9 The geometric imperfection introduced at the bottom of the notch tip is one single cosine shaped wave with length $0.04R$ and amplitude $0.002R$, where R represents the

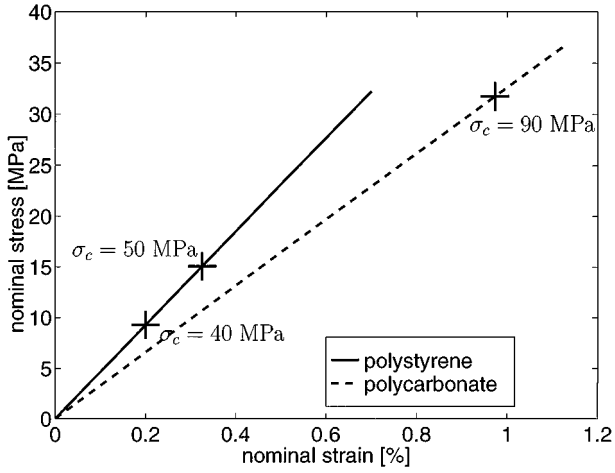

Figure 11 Nominal stress (defined with respect to the undeformed minimum cross-sectional area behind the notch tip) versus nominal strain of the notched test specimen, predicted for quenched polystyrene and polycarbonate material behaviour. The markers indicate the moment that the critical craze-initiation stress is reached.

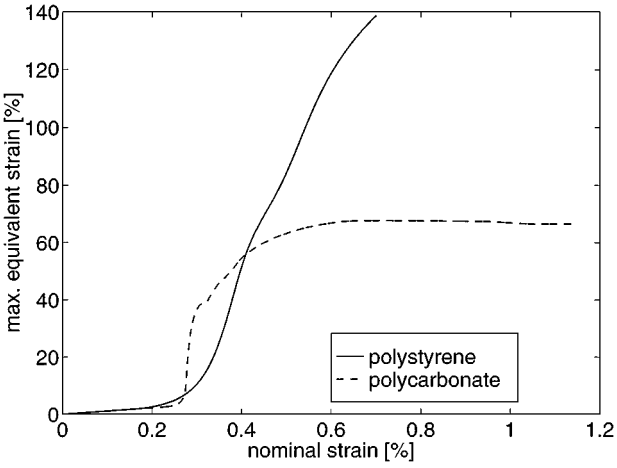

Figure 12 Maximum equivalent strain in the notched test specimen as a function of nominal (macroscopic) strain, predicted for quenched polystyrene and polycarbonate material behaviour.

notch tip radius. The finite element model is shown in Fig. 10. The plane strain mesh is composed of 8-node quadrilateral reduced integration elements and 6-node triangular elements. The element size is chosen such that the essential results presented in this section proved to be mesh independent[‡]. The specimen is loaded unidirectionally with a constant strain rate of 0.001 s^{-1}. In this strain rate region the temperature rise due to viscoplastic dissipation can be assumed to be negligible.

Fig. 11 shows the simulated predictions of the macroscopic mechanical responses of the polystyrene and polycarbonate tensile bars between 0 and 1.2% global strain. For this small-strain region the global responses are in fact linear elastic (Hooke's law) and thus comparable. The moduli differ because of the distinct shear moduli G (see Table I).

[‡] It is remarked that possible ill-posedness of the problem, associated with strain softening, disappears by the combined incorporation of considerable strain rate dependence of the yield stress and strain hardening (see Fig. 6), resulting in viscous regularisation [40], and stabilisation of the deformation, respectively. As a consequence, for a sufficiently fine finite element discretisation, the solution becomes independent of the particular mesh.

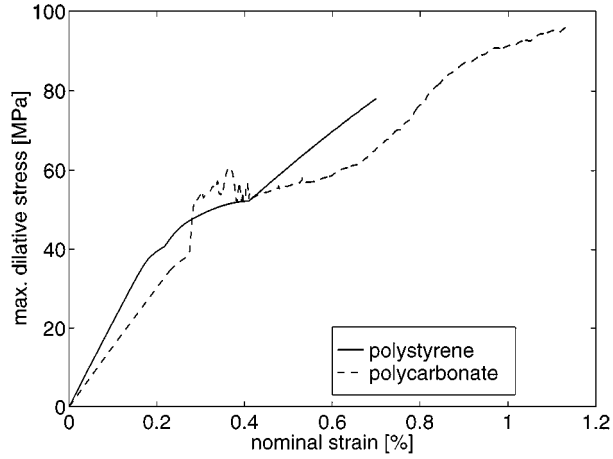

Figure 13 Maximum dilative stress in the notched test specimen as a function of nominal (macroscopic) strain, predicted for quenched polystyrene and polycarbonate material behaviour.

Figs 12 and 13 display the deformation processes occurring on a local scale: the maximum equivalent strain[§] and dilative stress as a function of the prescribed elongation. The sharp raise of the equivalent strain in a very early stage of the deformation process (nominal strain $\approx 0.3\%$) is obviously the result of local yielding, followed by strain softening. In fact, yielding already starts at a nominal strain of 0.16% in polystyrene and at 0.22% in polycarbonate, as could be deduced from a sudden increase of the local softening variable D at those strains.

A more detailed examination of the stress and strain fields behind the notch tip and defect at a global strain of 0.25%, visualised in Figs 14 and 15 respectively, reveals that the early yielding is triggered by the defect. Apparently, the stress concentrating defect causes yield, and the subsequent strain softening leads both to an acceleration of the (plastic) strain rate and a localisation of inelastic (and thus volume invariant) strains. As a result, a triaxial stress field is generated just below the surface of the defect. In both materials, the maximum dilative stress grows fast and for polystyrene the critical dilative stress of 40–50 MPa is reached between 0.2–0.32% global strain in a small material volume with a size of, approximately, 0.3 μm (which is large enough to accommodate a complete craze structure). At this point, all the plastic flow is still localised at the defect, see Fig. 16. A sharp shear band is formed just behind the defect in both materials, giving rise to a strong increase of the equivalent strain, as is shown in Fig. 12. Notice the remarkable differences in the evolution of local strains in PS and PC: polystyrene features a smooth but unbounded strain increase, while polycarbonate exhibits a short but strong strain growth, followed by stabilisation (by strain hardening) at a nearly constant limiting value. The more gradual start of (inelastic) strain growth in the polystyrene is probably due to the smaller initial slope of the softening response and the stabilising effect

[§] The equivalent strain $\varepsilon_{\mathrm{eq}}$ equals a norm of the logarithmic strain tensor $\boldsymbol{E}$, according to $\varepsilon_{\mathrm{eq}} = \sqrt{\frac{2}{3}\boldsymbol{E}^{\mathrm{d}} : \boldsymbol{E}^{\mathrm{d}}}$

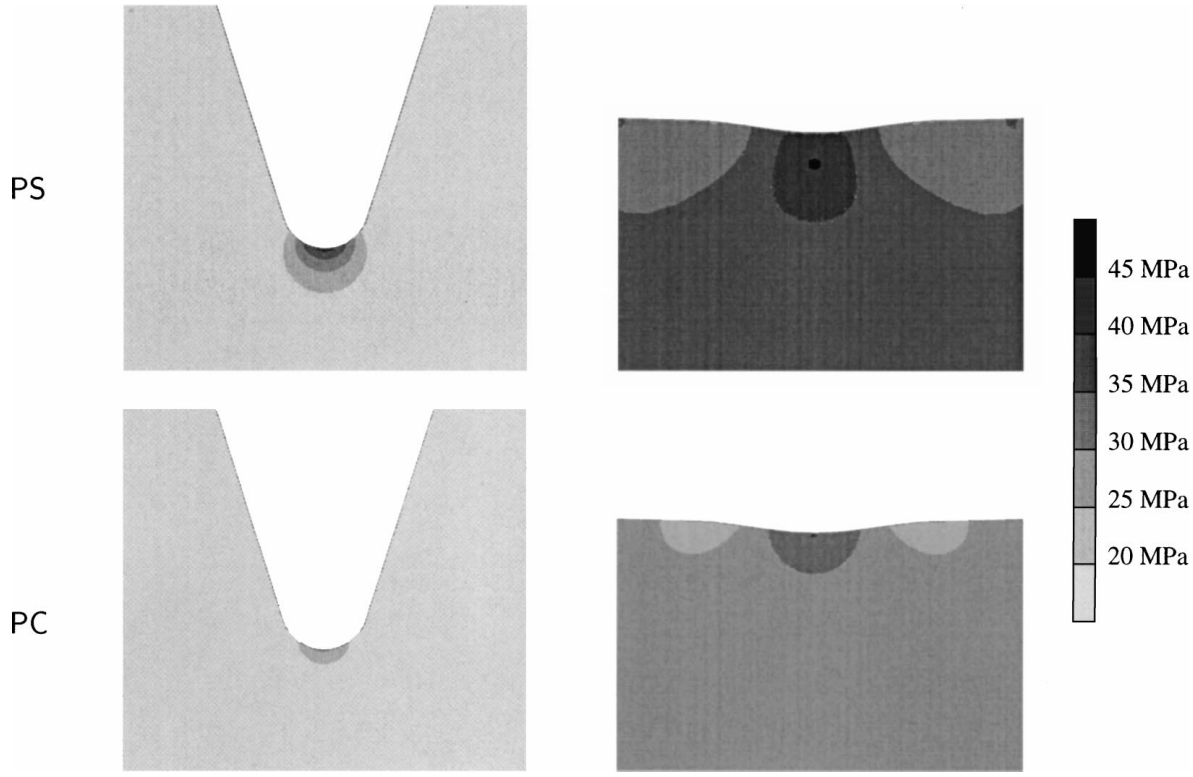

Figure 14 Contour plot of the dilative stress near the notch tip (left) and the defect (right) at a global strain of 0.25%, predicted for polystyrene (top) and polycarbonate (bottom) material behaviour.

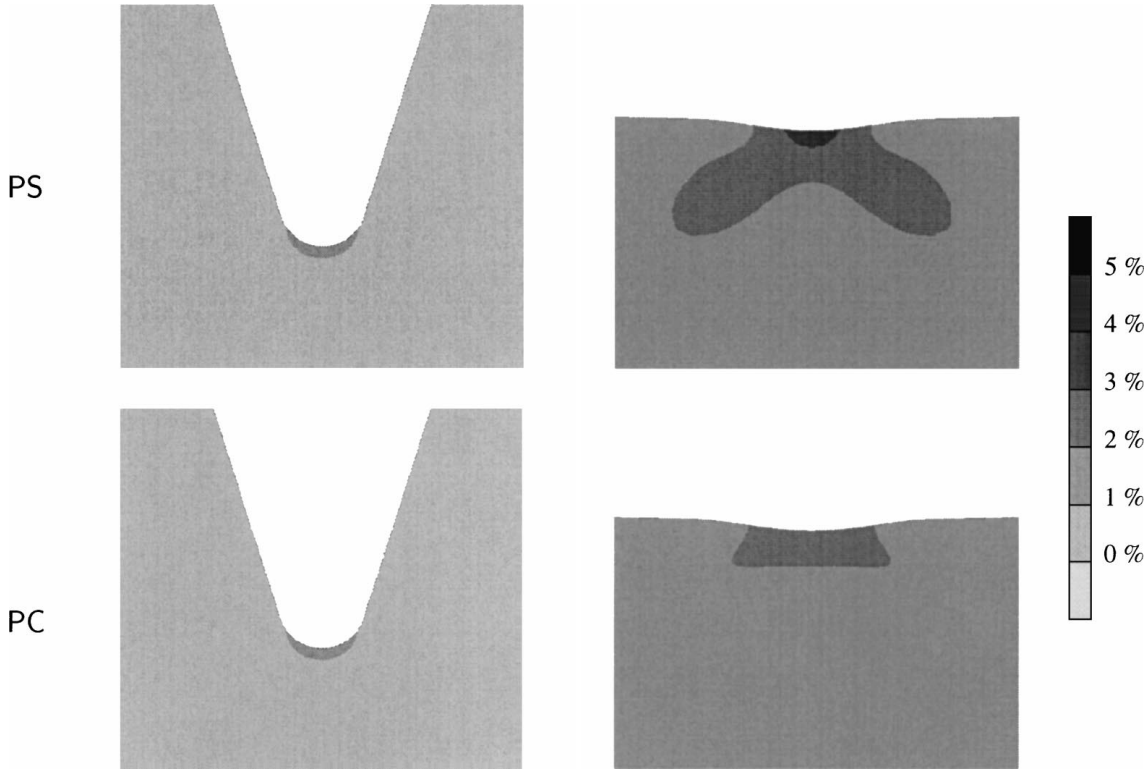

Figure 15 Contour plot of the equivalent strain near the notch tip (left) and the defect (right) at a global strain of 0.25%, predicted for polystyrene (top) and polycarbonate (bottom) material behaviour. Strains up to approximately 3% can be considered as being elastic.

of the strong strain rate dependence of the yield stress (compare Figs 6 and 7), while the unbounded growth is obviously the result of insufficient strain hardening. The sudden development of the sharp shear band in the polycarbonate also affects the local stress state, leading to some fluctuations in the maximum dilative stress, as shown in Fig. 13.

As the deformation proceeds, the effect of the stress-concentrating notch tip becomes more pronounced. Between 0.4 and 1% global strain, the dilative stress zone moves from the defect to eventually a position well below the notch tip, see, for polycarbonate, Fig. 17. This is accompanied by a strong dilative stress increase (see Fig. 13) up to unrealistic values for polystyrene. In the

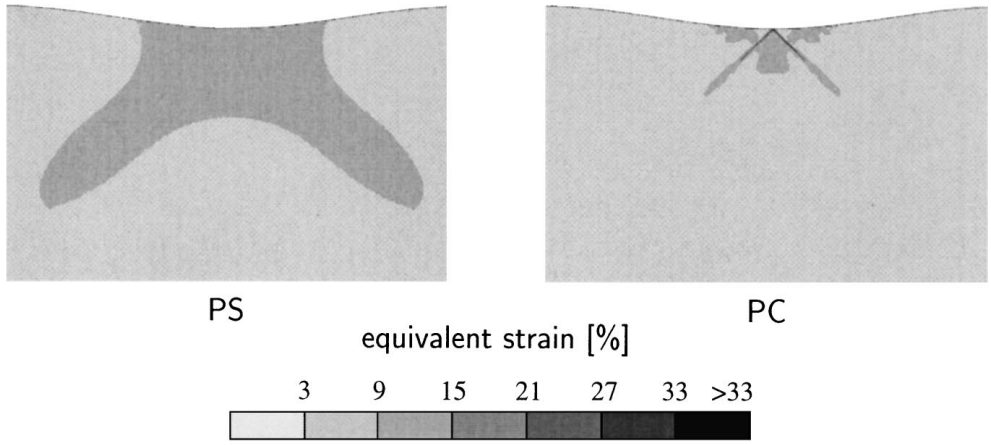

Figure 16 Contour plot of the equivalent strain below the defect at a global strain of 0.3%, predicted for polystyrene and polycarbonate material behaviour.

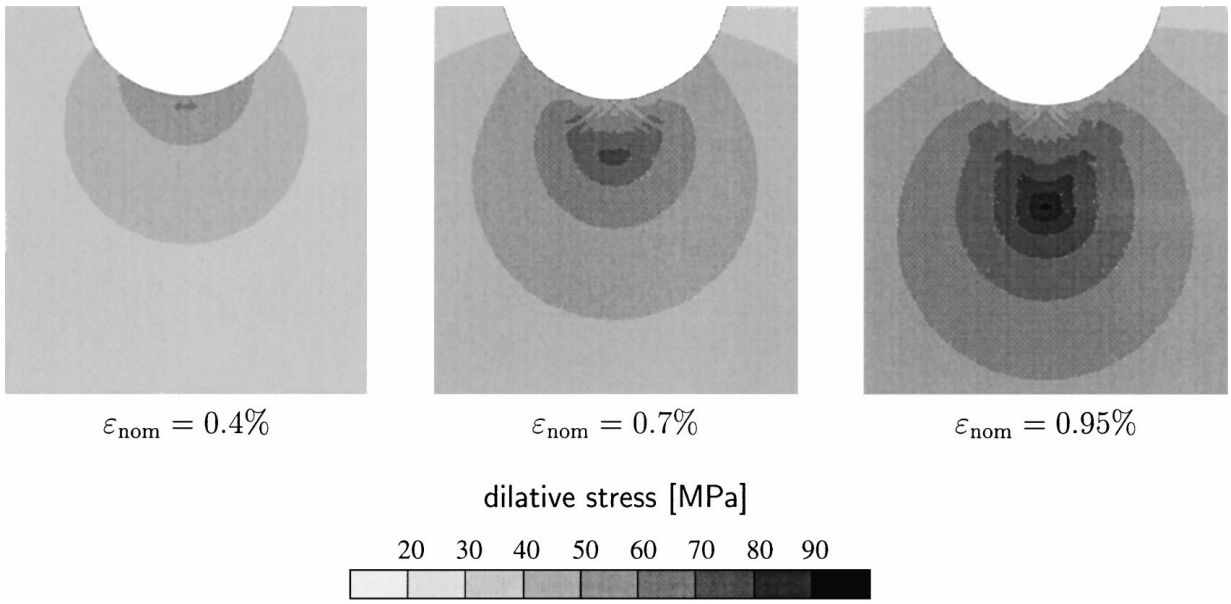

Figure 17 Contour plots of the dilative stress at different stages in the deformation process (0.4, 0.7, and 0.95% nominal strain), predicted for polycarbonate material behaviour.

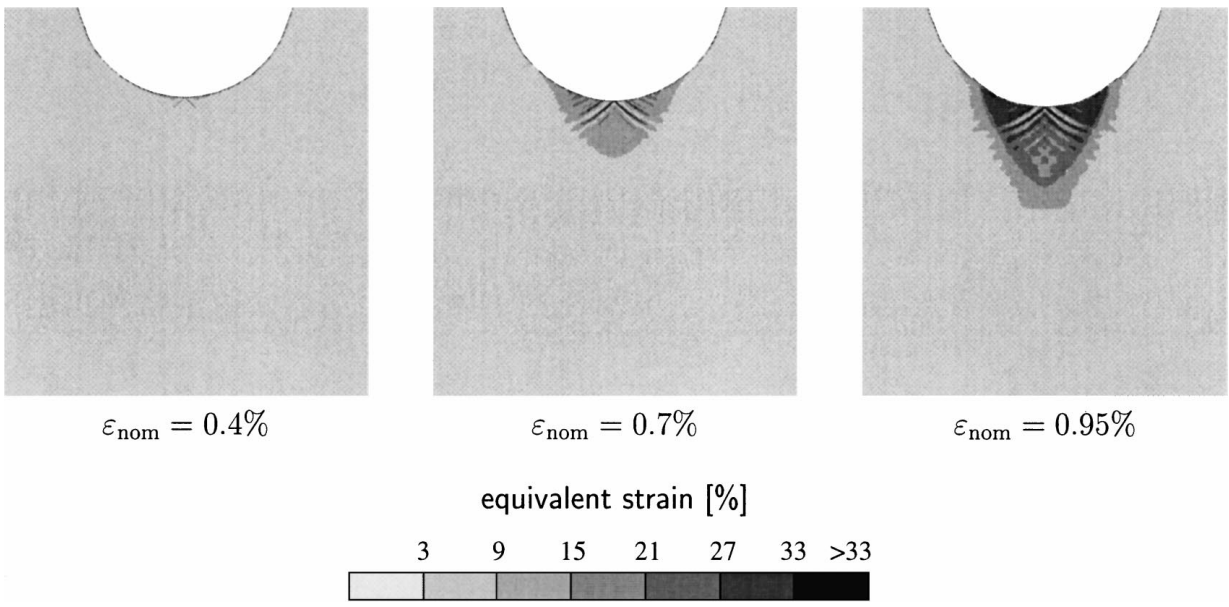

Figure 18 Contour plots of the equivalent strain at different stages in the deformation process (0.4, 0.7, and 0.95% nominal strain), predicted for polycarbonate material behaviour. Strains smaller than 3% are, approximately, elastic.

case of polycarbonate, however, the maximum strain stabilises by strain hardening (see Fig. 13) and reaches a constant, safe value of 65%. Fig. 18 shows the evolution of the equivalent strain field at the root of the notch, which consists of a large number of intersecting shear bands inclined along slip planes, similar to the experimental observations reported by Narisawa and Yee [32] and the numerical results of Lai and van der Giessen [41]. At a macroscopic strain of 0.95%, the critical dilative stress of 90 MPa is reached for the polycarbonate specimen. By then, the (stabilised) stress and strain fields near the defect are not critical anymore and the dilative stress region (which is in fact the craze nucleation zone) is positioned at a considerable distance from the bottom of the notch, far from the defect (see Fig. 17).

6. Discussion and conclusions

The results of the analyses show that polystyrene suffers from a combined unstable post-yield behaviour and a low craze-initiation resistance. Its unstable behaviour results in critical dilative stresses near small flaws or defects. Since critical dilative stresses are believed to be primarily responsible for craze initiation, often followed by fast unstable crack propagation, it is concluded that polystyrene is extremely defect sensitive and, therefore, brittle. Polycarbonate, on the other hand, appears to be tough, because its more pronounced strain hardening and better craze resistance diminish the effects of small imperfections. Polycarbonate, however, is notch sensitive because its critical dilative stress is still reached behind a notch. It is remarked that those results confirm Kramer's explanation for the brittleness of polymeric materials [1].

In this paper, it has been shown that the rather ambiguous qualifications 'brittle' and 'tough' depend on (i) the post-yield intrinsic mechanical behaviour of the materials, which is in fact the microstructural response, and (ii) the local dilative stress in the macrostructure, which follows from the local (intrinsic, microstructural) mechanical response and macroscopic geometry and loading conditions. For the homogeneous glassy polymers considered in this paper it was possible to use a relatively simple constitutive equation (a generalised compressible single-mode Leonov model) as a substitute for the microstructural response. For heterogeneous materials, however, a closed-form constitutive equation is not readily available. Therefore, a generally applicable homogenisation method was presented [13] that indeed generates the microstructural response from (a finite element model of) the microstructure, in order to obtain a reliable prediction of both macro and micro deformations for arbitrary shaped and loaded heterogeneous polymeric systems. Part II of this series of three papers [15] employs this novel micro-macro coupling method to analyse the effect of microstructural modifications on the macroscopic mechanical response. The consequences of the altered macroscopic behaviour for defect and notch sensitivity of notched tensile bars is investigated in the last Part III [16].

Acknowledgements

The authors wish to acknowledge the financial support provided by the Dutch Technology Foundation (STW) (Grant EWT.3766).

References

1. E. J. KRAMER, in "Adv. in Polymer Sci., Vol. 52/53," edited by H. H. Kausch (Springer-Verlag, Berlin, 1983) Ch. 1.
2. C. S. HENKEE and E. J. KRAMER, *J. Polym. Sci. Polym. Phys. Ed.* **22** (1984) 721.
3. E. J. KRAMER and L. L. BERGER, in "Adv. in Polymer Sci., Vol. 91/92," edited by H. H. Kausch (Springer-Verlag, Berlin, 1990) Ch. 1.
4. R. A. W. FRASER and I. M. WARD, *J. Mater. Sci.* **12** (1977) 459.
5. M. C. M. VAN DER SANDEN, J. M. M. KOK and MEIJER, *Polymer* **35** (1994) 2995.
6. M. C. M. VAN DER SANDEN, L. G. C. BUIJS, F. O. DE BIE and H. E. H. MEIJER, *ibid.* **35** (1994) 2783.
7. M. C. M. VAN DER SANDEN, H. E. H. MEIJER and P. J. LEMSTRA, *ibid.* **34** (1993) 2148.
8. B. J. P. JANSEN, H. E. H. MEIJER and P. J. LEMSTRA, *Polymer*, submitted.
9. A. M. L. MAGALHÃES and R. J. M. BORGGREVE, *Macromolecules* **28** (1995) 5841.
10. D. H. ENDER and R. D. ANDREWS, *Polymer Letters* **36** (1965) 3057.
11. T. A. TERVOORT, PhD thesis, Eindhoven University of Technology, Eindhoven, The Netherlands, 1996.
12. B. J. P. JANSEN, PhD thesis, Eindhoven University of Technology, Eindhoven, The Netherlands, 1998.
13. R. J. M. SMIT, W. A. M. BREKELMANS and H. E. H. MEIJER, *Comput. Methods Appl. Mech. Engrg.* **155** (1998) 181.
14. *Idem., J. Mech. Phys. Solids* **47** (1999) 201.
15. *Idem., J. Mater. Sci.* **35** (2000) 2869.
16. *Idem., ibid.* **35** (2000) 2881.
17. O. A. HASAN, M. C. BOYCE, X. S. LI and S. BERKO, *J. Polymer Sci.: Part B: Polymer Phys.* **31** (1993) 185.
18. P. H. M. TIMMERMANS, PhD thesis, Eindhoven University of Technology, Eindhoven, The Netherlands, 1997.
19. T. A. TERVOORT, R. J. M. SMIT, W. A. M. BREKELMANS and L. E. GOVAERT, *Mech. of Time Dep. Mat.* **1** (1997) 269.
20. M. C. BOYCE, D. M. PARKS and A. S. ARGON, *Mechanics of Materials* **7** (1988) 15.
21. *Idem., Int. J. Plasticity* **5** (1989) 593.
22. E. M. ARRUDA and M. C. BOYCE, *ibid.* **9** (1993) 697.
23. P. D. WU and E. VAN DER GIESSEN, *ibid.* **35** (1993) 935.
24. T. A. TERVOORT, E. T. J. KLOMPEN and L. E. GOVAERT, *J. Rheol.* **40** (1996) 779.
25. A. I. LEONOV, *Rheol. Acta* **15** (1976) 85.
26. F. P. T. BAAIJENS, *ibid.* **30** (1991) 284.
27. MARC, "Programmer and User Manuals" (MARC Analysis Research Corporation, Palo Alto, CA, USA, 1997).
28. R. J. M. SMIT, W. A. M. BREKELMANS and F. P. T. BAAIJENS, *Int. J. Numer. Methods Engrg.*, submitted.
29. G. M. GUSLER and G. B. MCKENNA, *Polym. Eng. Sci.* **37** (1997) 1442.
30. L. E. GOVAERT and T. PEIJS, *Mech. of Time Dep. Mat.*, submitted.
31. M. ISHIKAWA, H. OGAWA and I. NARISAWA, *J. Macromol. Sci.-Phys.* **B19** (1981) 421.
32. I. NARISAWA and A. F. YEE, in "Materials Science and Technology. A Comprehensive Treatment, Vol. 12," edited by E. L. Thomas (VCH, Weinheim, 1993) p. 699.
33. I. NARISAWA, M. ISHIKAWA and H. OGAWA, *J. Mater. Sci.* **15** (1980) 2059.
34. R. HILL, "The Mathematical Theory of Plasticity" (Oxford Univ. Press, London, 1950).
35. R. P. NIMMER and J. T. WOODS, *Polym. Eng. Sci.* **32** (1992) 1126.

36. L. E. GOVAERT and T. A. TERVOORT, in Proc. 9th Int. Conf. Def., Yield and Fracture of Polymers, Churchill College, Cambridge (The Institute of Materials, London, 1994) P67/1.
37. C. J. G. PLUMMER and A. M. DONALD. *J. Polym. Sci. Polym. Phys. Ed.* **27** (1989) 325.
38. M. ISHIKAWA, Y. SATO and H. HIGUCHI, *Polymer* **37** (1996) 1177.
39. S. HAVRILIAK, C. A. CRUZ and S. E. SLAVIN, *Polym. Eng. Sci.* **36** (1996) 2327.
40. J. C. SIMO, in "Cracking and Damage: Strain Localization and Size Effect," edited by J. Mazars and Z. P. Bažant (Elsevier, London 1989) p. 440.
41. J. LAI and E. VAN DER GIESSEN. *Mechanics of Materials* **25** (1997) 183.

Received 25 August 1998
and accepted 19 November 1999